5G Massive MIMO Architectures: Self-Backhauled Small Cells versus Direct Access

Andrea Bonfante, Lorenzo Galati Giordano, David López-Pérez, Adrian Garcia-Rodriguez, Giovanni Geraci, Paolo Baracca, M. Majid Butt, and Nicola Marchetti

***Abstract*—In this paper, we focus on one of the key technologies for the fifth-generation wireless communication networks, massive multiple-input-multiple-output (mMIMO), by investigating two of its most relevant architectures: *1)* to provide in-band wireless backhauling to a dense deployment of self-backhauled small cells (SCs) acting as communication relays to end-users, and *2)* to provide direct wireless access (DA) to end-users. Through comprehensive 3GPP-based system-level simulations and analytical formulation, we show the end-to-end user rates achievable with these two architectures. Different from the existing work, we provide results for two strategies of self-backhauled SCs deployments, namely *random* and *ad-hoc*. Where in the latter SCs are purposely positioned close to UEs to achieve line-of-sight (LoS) access links. We also show the optimal backhaul and access time resource partition due to the in-band self-backhauling operations. For the mMIMO DA, we consider the implication of different pilot reuse schemes for the channel state information (CSI) acquisition, associated overhead and contamination effects. We find that the ad-hoc deployment of self-backhauled SCs closer to the users (UEs) with optimal resource partition and with directive antenna patterns, provides rate improvements for cell-edge UEs that amount to 30%, and a tenfold gain as compared to mMIMO DA architecture with pilot reuse 3 and reuse 1, respectively. On the other hand, mMIMO s-BH underperforms mMIMO DA above the median of the UE rates when the UEs are in the center of the cell, and the effect of pilot contamination is mitigated.**

***Index Terms*—5G mobile communication, massive MIMO, wireless backhaul, small cell deployment, network capacity.**

I. Introduction

FIFTH-generation (5G) wireless communication systems are expected to support a 1000x increase in capacity compared to existing networks [2]. Meeting this gargantuan target will require mobile network operators (MNOs) to leverage new technologies, such as massive multiple-input-multiple-output (mMIMO), and to deploy a large number of additional small cells base stations (SCs) [3], [4]. Wireless self-backhauling (s-BH), achieved through the tight integration of these two complementary technologies, lures MNOs with the potential of achieving the desired capacity boost at a contained investment [5]. Indeed, exploiting the large number of spatial degrees-of-freedom available with mMIMO to provide sub-6 GHz in-band wireless backhauling to SCs offers multiple advantages to MNOs: *i)* avoiding deployment of an expensive wired backhaul infrastructure, *ii)* availing of more flexibility in the deployment of SCs, and *iii)* not having to purchase additional licensed spectrum, as in the case of out-of-band wireless backhauling [6].

Those advantages motivated the Third Generation Partnership Project (3GPP) to include in the 5G New Radio (NR) Release 15 a new study item, which focuses on Integrated Access and Backhaul (IAB) network architectures – also refereed to as *self-backhauling* networks in the literature. In [7], 3GPP provides a list of use cases, in both the sub-6 GHz and above-6 GHz spectrum bands, and network architecture requirements for the NR backhauling functionalities coupled with the radio access network (RAN) technology.

A. Background and related work

Several works focused on millimeter wave (mmWave) s-BH networks [8], [9], which offer wide bandwidth channels to accommodate multiple backhaul and access links simultaneously. At the same time, various research efforts considered sub-6 GHz s-BH networks in a heterogeneous network (HetNet) environment [10]–[12], which is more suitable to provide wide-area coverage through conventional macro-cells, and use self-backhauled SCs to further boost the network capacity. However, due to the scarcity of spectrum in the bands below 6 GHz, the bandwidth splitting required to serve multiple backhaul links and the inter-tier interference caused by co-channel access and backhaul operations may turn out to be a significant impediment to the potential adoption of s-BH in sub-6 GHz HetNets [12]. In [10], [11], the authors tackled the problem of resource allocation (such as transmission power and time-frequency resources) of s-BH networks. In [12], the authors considered full-duplex (FD) SCs, which avoid backhaul and access spectrum orthogonalization due to the possible bi-directional transmission, it is important to note that they require self-interference cancellation capabilities to prevent coverage degradation.

Moreover, works such as [13], [14], considered macro BSs equipped with mMIMO to enhance the backhaul link capacity and simultaneously serve SCs and user equipments (UEs). In [13], the authors studied the UE data-rate performance as a function of the distance between the mMIMO-BS and the s-BH SCs. However, they considered a simplified single-cell

This work was supported in part by Irish Research Council, by Nokia Ireland Ltd under Grant Number EPSPG/2016/106, and by Science Foundation Ireland (SFI) under the European Regional Development Fund – Grant Number 13/RC/2077.

A part of this paper is accepted for presentation at IEEE Globecom 2018 Wireless Communications Symposium in Abu Dhabi [1].

A. Bonfante (e-mail:andrea.bonfante.ext@nokia-bell-labs.com), L. Galati Giordano, D. López-Pérez, A. Garcia-Rodriguez, and G. Geraci are with Nokia Bell Labs Ireland. P. Baracca is with Nokia Bell Labs Germany. M. M. Butt is with University of Glasgow. N. Marchetti is with CONNECT Centre and the Department of Electronic & Electrical Engineering, Trinity College Dublin, Ireland. A. Bonfante is also with CONNECT Centre and Trinity College Dublin.

scenario without inter-cell interference between SCs. In [14], [15], the authors used stochastic geometry to derive the rate coverage probability and compute the optimal proportion of in-band and out-of-band FD SCs in the network which maximize the UE rates, and energy efficiency, respectively. Finally, the authors in [16] investigated an optimization approach to maximize the sum-rate of the UEs under capacity constrained backhaul and by considering the length of the pilot sequences used for the channel state information (CSI) acquisition.

B. Motivation and contribution

In this paper, we analyze the end-to-end UE performance of mMIMO s-BH architecture by means of theoretical analysis and 3GPP-based system-level simulations when compared to mMIMO Direct Access (DA), where mMIMO-BSs are solely dedicated to serving UEs in the absence of SCs [17]. We consider a realistic multi-cell setup [18], where mMIMO-BSs provide sub-6 GHz backhauling to a plurality of half-duplex (HD) SCs overlaying the macro cellular area. In these HD systems, a s-BH network entails sharing time-and-frequency resources between radio access and backhaul links. The analysis is necessary to understand the asymptotic behavior of the system, which cannot be simulated for computational complexity, whereas accurate 3GPP-based system-level simulations are necessary due to the non-tractability of the problem, when realistic channel and interference models are considered. Two different strategies of self-backhauled SCs deployments are considered as illustrated in Fig. 1. We analyze a *random* deployment – where SCs are uniformly distributed over a geographical area –, and an *ad-hoc* deployment – where SCs are purposely positioned close to UEs to achieve line-of-sight (LoS) access links. Indeed, the latter type of deployment can be supported by future dynamic network infrastructures, for example based on the applications of unmanned aerial vehicles (UAV) to carry SCs [19].

The contributions of the paper are as follows:

1) We provide 3GPP-based system-level simulations results on the performance of the achievable UE data-rates in mMIMO based wireless in-band s-BH with random and ad-hoc SCs deployments. To the best of the authors knowledge, we also compare for the first time the performance of mMIMO s-BH and mMIMO DA architectures. Differently from the previous works [13]–[16], our work accounts for a path loss model with LoS and Non-LoS (NLoS) transition regions in both backhaul and access links. Moreover, we consider the pilot contamination effect on the signal-to-interference-plus-noise ratio (SINR), when mMIMO is used. Both the path loss models incorporating LoS and NLoS transmissions and the pilot contamination effect severely impact the inter-cell interference modeling and simulation, and consequently the system performance.
2) We provide an analytical model for evaluating the average data-rate of the backhaul and access links. We adapt the expressions proposed in [20], [21] to model the mMIMO backhaul links. Specifically, we account for the effects of the antenna directionality and sectorization, and the effect of the beamforming gain due to the mMIMO precoding. In the access link formulation, we account for the density of active SCs, which matches the numerical results obtained by simulations. We also employ the analytical framework to show that, due to the over provisioning of self-backhauled SCs, random deployment requires thousands of SCs to achieve the same performance of the ad-hoc deployment.
3) We explain in details the different factors playing a key role in the 3GPP-based system-level results. Overall, the insights from these results can guide the deployment of the future 5G access network.

The remainder of this paper is organized as follows.[1] Section II introduces the system model on which the analysis is based; Section III presents the downlink (DL) SINR and rate expressions of the backhaul and access links; Section IV provides the analytical signal-to-interference ratio (SIR) and average rate expressions of backhaul and access; Section V presents the numerical results, and VI summarizes the key findings.

II. System model

We focus on the study of the DL performance for an hexagonal grid of mMIMO-BSs equipped with a large number of antennas M and providing wireless backhaul links to (a) randomly deployed self-backhauled SCs, (b) ad-hoc deployed self-backhauled SCs, or (c) directly serving UEs, as illustrated in Figs. 1(a), 1(b), and 1(c), respectively.

A. Macro cell, Small cell and user topologies

We denote by i, l, and k the mMIMO-BS in the i-th sector, the SC, and the UE, respectively. $\mathcal{I}$ represents the set of mMIMO-BSs deployed in the network. $\mathcal{L}_i$ and $\mathcal{L}_{i'}$ represent the set of SCs deployed per sector and connected to the i-th and i'-th mMIMO-BS, respectively, which provides the largest reference signal received power (RSRP).[2] L_i and $L_{i'}$ denote the number of SCs in the sets $\mathcal{L}_i$ and $\mathcal{L}_{i'}$, respectively. Furthermore, we denote by K_i the number of UEs randomly and uniformly distributed over the area covered by each sector. We assume that each single-antenna UE is connected with the SC (in the s-BH network), or with the mMIMO-BS (in the DA network) that provides the largest RSRP [18]. Therefore each SC serves K_l UEs in the s-BH network.

Three different network deployments are presented in the following:

(a) **s-BH architecture with random deployment:** Self-backhauled SCs are randomly and uniformly distributed over the mMIMO-BS geographical area, as shown in Fig. 1(a). This scenario is used as a baseline, and follows the set of parameters specified by the 3GPP in [18] to evaluate the relay scenario. More precisely, we consider

[1] Throughout the paper, capital and lower-case bold letters denote matrices and vectors, respectively, while $[\cdot]^*$, $[\cdot]^{\mathrm{T}}$ and $[\cdot]^{\mathrm{H}}$ denote conjugate, transpose, and conjugate transpose, respectively.

[2] We remark that a given SC deployed in the i-th sector might be connected to another mMIMO-BS i' as it provides a higher RSRP level than the mMIMO-BS i.

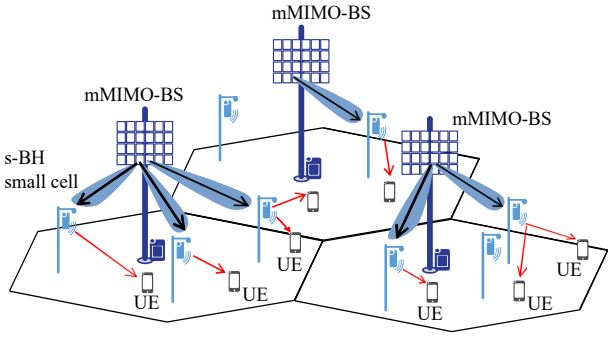

(a) s-BH architecture with random deployment

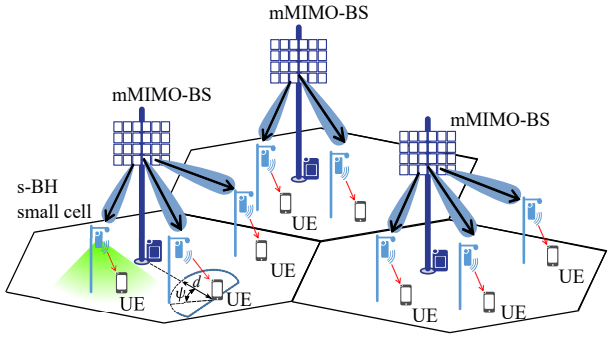

(b) s-BH architecture with ad-hoc deployment

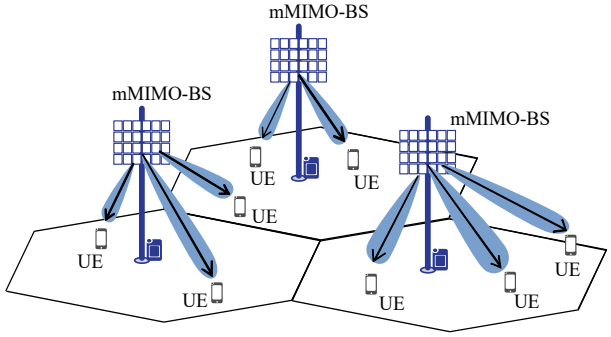

(c) DA architecture

Fig. 1: Illustration of (a) s-BH architecture with random deployment, (b) s-BH architecture with ad-hoc deployment, and (c) DA architecture.

the UE and SC antenna heights fixed at 1.5 and 5 meters above the ground, respectively, and channel models for the 3GPP Case 1 Relay scenario.

(b) **s-BH architecture with ad-hoc deployment:** Self-backhauled SCs are positioned targeting nearby UE locations.[3] As shown in Fig. 1(b), we model this scenario by considering SCs deployed within a 2-D (two-dimensional) distance d from the UEs, and an angle ψ measured from the straight segment that links UEs and their closest mMIMO-BS. ψ is chosen uniformly at random in $[-\pi/2, \pi/2]$. It is worth noting that even when the 2-D distance $d = 0$, UEs and SCs are still separated in space because the antennas are positioned at different heights, as specified in (a). In addition, to limit the effect of the inter-cell interference, we replace the Patch antenna at the SC with a more directive Yagi antenna, pointing downwards to the ground (as shown by the green radiation cone in Fig. 1(b)), and therefore only illuminating the closest UEs.

(c) **DA architecture:** There are no self-backhauled SCs deployed, and the mMIMO-BSs are solely dedicated to directly serve the UEs, as illustrated in Fig. 1(c).

[3] We assume the possibility to realize this specific network deployment, for example by means of drone-BSs, where the drone-BSs can reposition themselves following the locations of UEs as suggested in [22]. Although mentioned, the drone-BSs use-case is not the focus of this paper, and it is left for future investigation.

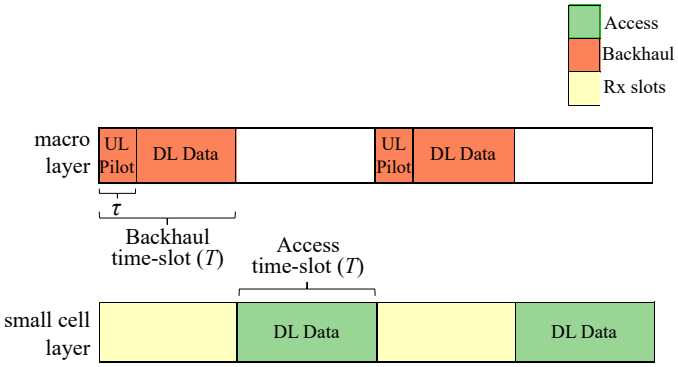

(a) Self-backhaul frame

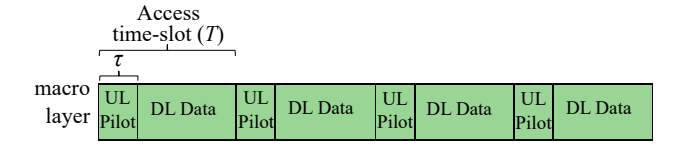

(b) Direct access frame

Fig. 2: DL frame structure for (a) mMIMO s-BH with $\alpha = 0.5$, and for (b) mMIMO DA.

B. Frame structure

We consider a time-division duplexing (TDD) system, where the time-slot duration T is used as a single scheduling unit in the time domain. As shown in Fig. 2(a), we partition the access and backhauling resources through the parameter $\alpha \in [0, 1]$. Therefore, the fraction α of time-slots is allocated to the backhaul links, and the fraction $1 - \alpha$ of time-slots is allocated to the access links. In the frequency domain, we divide the system bandwidth BW into Q_t RBs, and we allocate all the RBs to the backhaul links or the access links. We make the following assumptions in considering the partition of backhaul and access time-slots among the SCs and UEs:

- During the backhaul time-slots, all the associated SCs are served by the mMIMO-BS i, and we use the same value of α for all the SCs. The mMIMO-BSs precode the backhaul signals towards the single-antenna SCs, which are spatially multiplexed in the same time-frequency resources.
- During the access time-slots, the SCs schedule their connected UEs by using a Round Robin (RR) mechanism, which equally distributes the available Q_t RBs among its UEs.

Fig. 2(b) shows the frame structure used for the DA setup, where all the time-slots are allocated to the access links. In each time slot, the mMIMO BSs precode the access signals, and the UEs are spatially multiplexed reusing the entire system bandwidth.

Figs. 2(a) and 2(b) also show the fraction τ of the time-slots dedicated for the transmission of the uplink (UL) pilot sequences, used for the CSI acquisition. Details about the CSI acquisition procedure will be discussed in subsection II-D.

C. Channel model

We define as $\mathbf{h}_{il} = [h_{il1}, \ldots, h_{ilM}]^{\mathrm{T}} \in \mathbb{C}^M$ the propagation channel between the l-th single-antenna receiver (SC in the mMIMO s-BH network and UE in the mMIMO DA) and the M antennas of the i-th mMIMO-BS. The composite channel matrix between the i-th mMIMO-BS and the receivers in the i'-th cell is represented by $\mathbf{H}_{i,i'} = [\mathbf{h}_{i1} \cdots \mathbf{h}_{iL_{i'}}] \in \mathbb{C}^{M \times L_{i'}}$, where we omit the subscript q indicating the q-th RB of the channel matrix for notational convenience. Moreover, for the mMIMO sBH architecture, we define the single-input single-output (SISO) channel between the l-th SC and the k-th UE in the q-th RB as $g_{lkq} \in \mathbb{C}$.

The channel coefficients $h_{ilm} = \sqrt{\beta_{il}}\tilde{h}_{ilm}$ and $g_{lkq} = \sqrt{\beta_{lk}}\tilde{g}_{lkq}$ account for both the effects of the large-scale fading and the small-scale fading components:

- We model the large-scale fading components $\beta_{il}, \beta_{lk} \in \mathbb{R}^+$ according to the 3GPP Case 1 Relay scenario [18]. For a given link, the models decide whether the channel propagation conditions are LoS or NLoS, by considering a distance-dependent LoS probability function, and use log-normal distributed shadowing with different values of standard deviation. Because of its slow-varying characteristic, the large-scale fading does not change rapidly with time, and it can be assumed constant over the observation time-scale of the network.
- We model the small-scale fading components $\tilde{h}_{ilm}, \tilde{g}_{lkq} \in \mathbb{C}$, which result from multi-path, as Rician fast-fading, according to the 3GPP spatial channel model for MIMO simulations [23], assuming a K-factor dependent on the distance between transmitter and receiver.

Throughout the paper, we assume uncorrelated channel fading realizations for the SC-UE and the mMIMO-BS-UE links between successive time-slots and different RBs, while for the mMIMO-BS-SC link, we consider the backhaul channel constant for a period $T_{BH} \gg T$ due to the static position of the SCs.

D. Massive MIMO CSI acquisition

To calculate the DL precoder of the mMIMO-BS, we consider that the channel is estimated through UL pilot sequences, assuming UL/DL channel reciprocity [3]. We also consider that the SCs or UEs associated to the same mMIMO-BS have orthogonal pilot sequences, and define the pilot codebook with the matrix $\mathbf{\Phi}_i = [\boldsymbol{\phi}_{i1} \cdots \boldsymbol{\phi}_{iL_i}]^{\mathrm{T}} \in \mathbb{C}^{L_i \times B}$, which satisfies $\mathbf{\Phi}_i \mathbf{\Phi}_i^{\mathrm{H}} = \mathbf{I}_{L_i}$. Here, the l-th sequence is given by $\boldsymbol{\phi}_{il} = [\phi_{il1}, \ldots, \phi_{ilB}]^{\mathrm{T}} \in \mathbb{C}^B$, and B denotes the pilot codebook length. Note that $L_i \leq B$, i.e., the maximum number of SCs or UEs served by the mMIMO-BSs in a time-slot, is limited by the number of orthogonal pilot sequences.

The matrix $\mathbf{Y}_i \in \mathbb{C}^{M \times B}$ of pilot sequences received at the i-th mMIMO-BS can be expressed as [24]

$$\mathbf{Y}_i = \sqrt{P_{il}^{\mathrm{ul}}} \sum_{i' \in \mathcal{I}} \mathbf{H}_{i,i'} \mathbf{\Phi}_{i'} + \mathbf{N}_i, \tag{1}$$

where P_{il}^{ul} is the power used for UL pilot transmission by the l-th device, located in the i-th sector, and $\mathbf{N}_i \in \mathbb{C}^{M \times B}$ represents the additive noise matrix, whose entries are modeled as independent and identically distributed complex Gaussian random variables with variance σ^2.

Let us denote by $\mathbf{H}_i = [\mathbf{h}_{i1} \cdots \mathbf{h}_{iL_i}] \in \mathbb{C}^{M \times L_i}$ the channel between the i-th mMIMO-BS and the associated devices. During the UL training phase, the mMIMO-BS obtains an estimate of $\mathbf{H}_i$ by correlating the received signal with a known pilot matrix $\mathbf{\Phi}_i$. Let us define $\mathcal{P} \subseteq \mathcal{I}$ as the subset of sectors, whose devices share identical pilot sequences with the devices served by the i-th mMIMO-BS. The resulting least-squares (LS) channel estimation can be expressed as [25]

$$\widehat{\mathbf{H}}_i = \frac{1}{\sqrt{P_{il}^{\mathrm{ul}}}} \mathbf{Y}_i \mathbf{\Phi}_i^{\mathrm{H}} = \mathbf{H}_i + \sum_{i' \in \mathcal{P}} \mathbf{H}_{i,i'} + \frac{1}{\sqrt{P_{il}^{\mathrm{ul}}}} \mathbf{N}_i \mathbf{\Phi}_i^{\mathrm{H}}. \tag{2}$$

The first, second and third terms on the right-hand side of (2) represent the estimated channel, a residual pilot contamination component and the noise after the pilot sequence correlation, respectively. The use of the same set of orthogonal pilot sequences among different sectors leads to the well-known *pilot contamination* problem, which can severely degrade the performance of mMIMO systems [3], [26].

In mMIMO s-BH systems, since the coherence time of the backhaul channel T_{BH} is longer than the time-slot duration T, the backhaul pilot sequences for CSI acquisition can be transmitted less frequently than every T. In this paper, we consider multiplexing the mMIMO pilots transmitted by the SCs of different sectors over separate backhaul time-slots. Thus, providing pilot orthogonality in the entire network. Therefore, we account for the pilot transmission overhead, but we assume that no pilot contamination occurs for the mMIMO s-BH system. In contrast, for mMIMO DA, this assumption does not hold, and accordingly, we consider a maximum of 16 orthogonal pilot sequences multiplexed in each orthogonal frequency division multiplexing (OFDM) symbol as per [26]. Two pilot allocation schemes are compared here:

- *Pilot reuse 1 scheme (R1):* All K_i UEs per sector are trained in $\tau = 1$ OFDM symbol out of the total of 14 OFDM symbols.
- *Pilot reuse 3 scheme (R3):* The sectors of the same site use orthogonal pilot sequences. This scheme avoids pilot contamination from co-sited sectors, but requires $\tau = 3$ OFDM symbols out of the total of 14 OFDM symbols, resulting in a higher pilot overhead when compared to the R1 scheme.

The reuse scheme 1 allows the use of the minimum number of OFDM symbols to acquire the CSI of all the UEs, but leads to severe conditions of pilot contamination. Instead, the reuse scheme 3 reduces the effect of pilot contamination at

the expense of increasing three times the overhead required to transmit the pilot sequences [26].

III. Downlink SINR and User Rate

In this section, we present the formulation for the two-hop DL data-rate in the s-BH network, which comprises the formulation for the mMIMO backhaul and the SC access SINRs and data-rates. Moreover, we include the conventional formulation for the data-rates in mMIMO DA network.

A. Massive MIMO backhaul transmission

The i-th mMIMO-BS uses the precoding matrix $\mathbf{W}_i = [\mathbf{w}_{i1} \cdots \mathbf{w}_{iL_i}] \in \mathbb{C}^{M \times L_i}$ to serve its connected SCs during the backhaul time slot. In this paper, we consider that $\mathbf{W}_i$ is computed based on the zero-forcing (ZF) criterion as

$$\mathbf{W}_i = \mathbf{D}_i^{\frac{1}{2}} \widehat{\mathbf{H}}_i \left(\widehat{\mathbf{H}}_i^{\mathrm{H}} \widehat{\mathbf{H}}_i \right)^{-1}. \tag{3}$$

Here, the diagonal matrix $\mathbf{D}_i = \mathrm{diag}\left(\rho_{i1}, \rho_{i2}, \ldots, \rho_{iL_i}\right)$ is chosen to equally distribute the total DL power P_i^{dl} among the L_i receivers. In the previous expression, ρ_{il} represents the power allocated to the l-th receiver located in the i-th sector, and $\mathrm{Tr}\{\mathbf{D}_i\} = P_i^{\mathrm{dl}}$, where $\mathrm{Tr}\{\mathbf{D}_i\}$ is the trace of matrix $\mathbf{D}_i$.

Under the assumption that each SC has perfect CSI available, the DL SINR of the l-th stream transmitted by the i-th mMIMO-BS can be expressed as

$$\mathrm{SINR}_{il}^{\mathrm{B}} = \frac{\rho_{il} |\mathbf{h}_{il}^{\mathrm{H}} \mathbf{w}_{il}|^2}{\sum\limits_{\substack{j \in \mathcal{L}_i \\ j \neq l}} \rho_{ij} |\mathbf{h}_{il}^{\mathrm{H}} \mathbf{w}_{ij}|^2 + \sum\limits_{\substack{i' \in \mathcal{I} \\ i' \neq i}} \sum\limits_{j \in \mathcal{L}_{i'}} \rho_{i'j} |\mathbf{h}_{i'l}^{\mathrm{H}} \mathbf{w}_{i'j}|^2 + \sigma_n^2}. \tag{4}$$

The numerator of (4) contains the power of the signal intended for the l-th receiver, and the denominator includes the intra-cell interference from the serving i-th mMIMO-BS, the inter-cell interference from other mMIMO-BSs, and the power of the thermal noise at the SC receiver σ_n^2.

The corresponding DL backhauling rate at the l-th SC receiver can therefore be expressed as

$$R_{il}^{\mathrm{B}} = \alpha \left(1 - \frac{\tau}{T}\right) BW \log_2 \left(1 + \mathrm{SINR}_{il}^{\mathrm{B}}\right). \tag{5}$$

where α, as indicated before, represents the fraction of time-slots allocated to the backhaul links.

B. Small cell access transmission

We recall from the channel model that g_{lkq} denotes the SISO channel between the l-th SC and the k-th UE corresponding to the q-th RB. The DL SINR of the k-th UE served by the l-th SC in RB q can be expressed as

$$\mathrm{SINR}_{lkq}^{\mathrm{A}} = \frac{P_l^{\mathrm{dl}} |g_{lkq}|^2}{\sum\limits_{i \in \mathcal{I}} \sum\limits_{\substack{l' \in \mathcal{L}_i \\ l' \neq l}} P_{l'}^{\mathrm{dl}} |g_{l'kq}|^2 + \sigma_{n_2}^2}, \tag{6}$$

where P_l^{dl} and $P_{l'}^{\mathrm{dl}}$ are the transmit powers on the RB of the l-th and l'-th SCs, respectively, and $\sigma_{n_2}^2$ denotes the thermal noise power at the UE receiver.

The corresponding DL access rate for UE k served by SC l can be therefore expressed as

$$R_{lk}^{\mathrm{A}} = (1 - \alpha) \frac{BW}{Q_t} \sum_{q=1}^{Q_t} x_q^k \log_2 \left(1 + \mathrm{SINR}_{lkq}^{\mathrm{A}}\right), \tag{7}$$

where $x_q^k = 1$ if the q-th RB is assigned to the k-th UE, and $x_q^k = 0$ otherwise.

The potential aggregated DL access rate provided by the l-th SC is $R_l^{\mathrm{A}} = \sum_{k=1}^{K_l} R_{lk}^{\mathrm{A}}$. However, the actual aggregated DL access rate provided by the l-th SC cannot be larger than the backhaul DL rate, which entails that $R_l^{\mathrm{A}} \leq R_{il}^{\mathrm{B}}$, $\forall l \in \mathcal{L}_i$, and $\forall i \in \mathcal{I}$. In this paper, we assume that the backhaul capacity is equally divided between the K_l UEs served by the l-th SC.[4] Therefore, the resulting end-to-end access rate for the k-th UE can be expressed as

$$R_{ilk} = \min \left(\frac{R_{il}^{\mathrm{B}}}{K_l}, R_{lk}^{\mathrm{A}} \right). \tag{8}$$

C. Massive MIMO direct access transmission

In contrast to s-BH setups, mMIMO systems providing DA dedicate all their time resources to multiplex DL data streams to the UEs. Thus, the DL access rate of the k-th UE served by the i-th mMIMO-BS can be expressed as

$$R_{ik}^{\mathrm{DA}} = \left(1 - \frac{\tau}{T}\right) BW \log_2 \left(1 + \mathrm{SINR}_{ik}^{\mathrm{DA}}\right), \tag{9}$$

where the estimated channel matrix $\widehat{\mathbf{H}}_i = [\widehat{\mathbf{h}}_{i1} \cdots \widehat{\mathbf{h}}_{iK_i}] \in \mathbb{C}^{M \times K_i}$ between the i-th mMIMO-BS and its connected UEs is plugged into (3), to subsequently derive the DL SINR in (4), assuming that each UE has perfect CSI available, and the access rate in (9).

IV. Analytical SIR and average backhaul and access Rates

In the following, we present a tractable formulation to model the mMIMO s-BH network, which approximates the backhaul and access SINR and data-rate expressions.

We recall from Section II that mMIMO-BSs are positioned in deterministic locations based on the hexagonal grid model. λ_a represents the density of mMIMO-BSs, and is calculated for the tri-sectorized deployment as $\lambda_a = 3(\frac{3\sqrt{3}}{2} R^2)^{-1}$, where $R = \frac{d_{ISD}}{\sqrt{3}}$ is the outer sector radius of the hexagonal site, and d_{ISD} is the inter-site distance between two hexagonal sites. For the random deployment of SCs, we consider modeling the locations of the s-BH SCs and UEs as two independent homogeneous Poisson Point Processes (PPPs) with densities λ_b and λ_u, respectively. For the ad-hoc deployment, we recall from the system model that the SCs are positioned nearby the locations of UEs. Thus, the SCs are distributed in the same way as the UEs, which are PPP distributed. The density of SCs

[4] The assumption of equally distributed backhaul capacity among the UEs might become a drawback for the end-to-end rates, when UEs served by the same SC have different rate requirements in the access links, and in this case, the partition of the backhaul resources among the UEs could be designed according to their demands. This access-based partition of the backhaul resources among the UEs is not the focus of this paper, and its study in the context of s-BH architecture is left for future work.

is calculated as $\lambda_b = 3L_i(\frac{3\sqrt{3}}{2}R^2)^{-1}$, where L_i is the number of small-cells per sector. The density of UEs is calculated as $\lambda_u = 3K_i(\frac{3\sqrt{3}}{2}R^2)^{-1}$, where K_i is the number of UEs per sector. When the SCs are deployed randomly within the sector area, there is a probability that some of them will not have any UE associated, since UEs connect to the SC with shortest path loss distance. This probability can be approximated as [27]

$$p_a \approx 1 - \left(1 + \frac{\lambda_u}{3.5\lambda_b}\right)^{-3.5}. \quad (10)$$

Therefore we approximate the number of active SCs as $L_a \approx p_a L_i$, and we omit the subscript i for notational convenience. The subset of active SCs is also assumed to follow a PPP process [27], and thus we can define the density of active SCs as $\tilde{\lambda_b} \approx p_a\lambda_b$. In the following expressions, SIR is used to approximate the SINR, since in the sub-6 GHz bands, with a system design which assures signal coverage, the system operates in interference-limited conditions, where the power of received interference dominates the denominator of the SINR.

A. Average rates of massive MIMO backhaul transmission

We now provide an analytical model for evaluating the average data-rate of the backhaul links, given the SIR of a typical SC and the spatial distribution of SCs in the sector. Inspired by [21], we treat the SCs as UEs, and we extend the framework proposed in [20] to model the SIR by considering: *i)* the effects of antenna directionality and sectorization, captured with the horizontal and vertical antenna patterns, and by modeling the co-site interference component; *ii)* the effect of the beamforming gain due to the mMIMO precoding as proposed in [14]. We make the following assumptions in our analytical backhaul model:

- For simplicity, the backhaul channel is statistically modeled by considering only the large-scale fading component, excluding shadowing statistics.
- We assume LoS propagation channel conditions from the serving mMIMO-BS to the SC (and from the co-site interfering mMIMO-BSs to the SC), to reflect the characteristics of the backhaul link, which tends to have dominant LoS conditions between SCs and the antennas of the nearest mMIMO-BSs [18]. On the other hand, we assume all the mMIMO-BSs from the surrounding interfering sites to be in NLoS.
- We assume that the co-channel interference from the mMIMO-BS to other served SCs can be reasonably neglected, since we adopt the ZF precoder, and we consider ideal CSI acquisition.

For the analysis that follows, r and θ denote two independent random variables (RVs), which define the distance and the angle from the SC to the serving mMIMO-BS. Note that r and θ are distributed with uniform probability density functions (pdfs) $f_R(r)$ and $f_\Theta(\theta)$ in the interval $[r_{\min}, \frac{d_{ISD}}{2}]$ and $[-\pi/3, +\pi/3]$, respectively, where the distance $r_{\min}$ denotes the minimum distance between the mMIMO-BS and the SC. By convention, $\theta = 0$ indicates the boresight direction in the first sector, and such sector is denoted as $s = 1$ for each hexagonal cell formed by S sectors.

The SIR of a typical SC associated to the mMIMO-BS is approximated as

$$\mathrm{SIR}^{\mathrm{B}}(r,\theta) \approx \frac{(M - L_a + 1)}{L_a} \frac{P_i^{\mathrm{dl}} G_a G_V(r) G_{H,1}(\theta) \beta^{\mathrm{L}}(r)}{I_1(r,\theta) + I_2(r)}, \quad (11)$$

where the multiplying factor $[(M - L_a + 1)]/L_a$ represents the beamforming gain from mMIMO precoding.[5] G_a, $G_V(r)$ and $G_{H,s}(\theta)$ are the antenna gains of the single mMIMO-BS element, the vertical (V), and the horizontal (H) antenna patterns, respectively. $\beta^{\mathrm{L}}(r) = A^{\mathrm{L}} r^{-\eta^{\mathrm{L}}}$ is the path loss between mMIMO-BS and SC, where A^{L} and η^{L} indicate the frequency dependent path loss factor and the the path loss exponent for the backhaul link in LoS condition, respectively, and $I_1(r,\theta)$ and $I_2(r)$ are the co-site and inter-site interference components, respectively. The vertical antenna pattern is defined as [18]

$$G_V(r)|_{\mathrm{dBi}} = -\min\left(12\left(\frac{\mathrm{atan}\left(\frac{\delta_a}{\sqrt{r^2 - \delta_a^2}}\right) - \zeta_{\mathrm{tilt}}}{\zeta_{HP}}\right)^2, F_v\right), \quad (12)$$

where δ_a is the difference in antenna heights between the mMIMO-BS and the SC, ζ_{tilt} is the mechanical downtilt, ζ_{HP} is the half-power vertical beamwidth, and F_v is the vertical front-back ratio. Similarly, the horizontal antenna pattern is defined as [18]

$$G_{H,s}(\theta)|_{\mathrm{dBi}} = -\min\left(12\left(\frac{\theta - (s-1)2\pi/3}{\theta_{HP}}\right)^2, F_h\right), \quad (13)$$

where θ_{HP} is the half-power horizontal beamwidth, and F_h is the horizontal front-back ratio.

In (11), $I_1(r,\theta)$ is represented as

$$I_1(r,\theta) = P_{i'}^{\mathrm{dl}} G_a G_V(r) \sum_{s=2}^{S} G_{H,s}(\theta) \beta^{\mathrm{L}}(r), \quad (14)$$

and $I_2(r)$ is approximated as [20]

$$I_2(r) \approx \frac{2\pi\lambda_a P_{i'}^{\mathrm{dl}} G_a G_V(2R_c - r)\overline{G_H} A^{\mathrm{NL}}}{\eta^{\mathrm{NL}} - 2} \times \left((2R_c - r)^{2-\eta^{\mathrm{NL}}} - (R_b - r)^{2-\eta^{\mathrm{NL}}}\right), \quad (15)$$

where $R_b = \frac{3}{2}d_{ISD}$ denotes the network boundary, $R_c = \frac{d_{ISD}}{2}$ is the inner sector radius, $\overline{G_H} = \int_0^{2\pi} \sum_{s=1}^{S} G_{H,s}(\theta) d\theta$ is the average horizontal antenna gain with respect to θ, and η^{NL} and A^{NL} are the path loss exponent and the frequency dependent path loss factor for the backhaul link in NLoS condition, respectively.

Finally, the average SC data-rate for backhaul transmission can be expressed as

$$\overline{R^{\mathrm{B}}} = \alpha\, BW \times \int_{-\frac{\pi}{3}}^{\frac{\pi}{3}} \int_{r_{\min}}^{R_c} \log_2\left(1 + \mathrm{SIR}^{\mathrm{B}}(r,\theta)\right) f_R(r) f_\Theta(\theta)\, dr\, d\theta. \quad (16)$$

[5] Only the L_a active SCs are spatially multiplexed in the backhaul timeslots, since those inactive are not required to backhaul the UEs data.

Therefore, the results for the average SC data-rate can be computed by numerical integration of (16).

B. Average rates of small cell access transmission

Inspired by the stochastic geometry analysis presented in [28], we now provide an analytical model for evaluating the access SIR of a typical UE and its access average DL data-rate. Similarly to [29], [30], we consider the impact of the LoS and NLoS path loss characteristics to model the SIR. We use the same LoS probability function as in [30], however, we consider for the inter-cell interference computation the density of the active SCs, i.e. those with UEs associated. Differently from [29], we consider that the serving SC always has a LoS path to the UE, due to the proximity of SC to UE. We will show by simulations in Fig. 3 that this approximation is realistic in the considered range of SCs densities.

We make the following assumptions in our analytical access model:

- We assume that each UE connects to the nearest SC, and the distance to the server x is Rayleigh distributed [28], with pdf $f_X(x) = 2\pi\lambda_b x \exp(-\lambda_b \pi x^2)/\exp(-\lambda_b \pi \delta_b^2)$, where δ_b denotes the difference between the SC and UE heights.
- The propagation channels are represented with a combination of distance-dependent path loss and multi-path fading, distributed as Rayleigh with an exponential power distribution $|g|^2 \sim \exp(1)$.[6]
- We adopt a probabilistic LoS channel model for the inter-cell interference, with a LoS probability expressed as [30]

$$\Pr^{\mathrm{L}}(x) = \exp(-(x/D)^2), \tag{17}$$

  where the parameter D is set to approximate the LoS probability of the SC-UE 3GPP model [30].

The SIR of a typical UE associated to the SC is approximated as

$$\mathrm{SIR}^{\mathrm{A}}(x) \approx \frac{P_l^{\mathrm{dl}} G_b |g|^2 \beta^{\mathrm{L}}(x)}{I_{\mathrm{agg}}}, \tag{18}$$

where G_b is the SC antenna gain, $|g|^2$ is the multi-path channel gain, and I_{agg} is the aggregated inter-cell interference.

We now use (18) to provide an expression for the rate coverage probability, which defines the probability that the UE rate is higher than a minimum target R_{th}. This probability can be expressed as $\Pr\left[\mathrm{SIR}^{\mathrm{A}}(x) > \gamma_a\right]$, where $\gamma_a = 2^{\frac{R_{th}}{\overline{K}-1}} - 1$ depends on R_{th}, and $\overline{K}$ is the average number of UEs served per SC, and is approximated using (10) as $\overline{K} \approx K_i/L_a$, which matches the numerical results show later in Fig. 5(b). The expressions used to evaluate the rate coverage probability are included in Appendix A. Thus, the average UE data-rate for access transmission can be expressed as

$$\overline{R^{\mathrm{A}}} = (1-\alpha)\, BW \times \int_0^{+\infty} \int_{\delta_b}^{+\infty} \Pr\left[\mathrm{SIR}^{\mathrm{A}}(x) > \gamma_a\right] f_X(x)\, dx\, d\gamma_a. \tag{19}$$

[6] Shadowing statistics are neglected in the analytical model, although a more comprehensive framework can incorporate this effect in the distribution of the UE distances.

TABLE I: 3GPP-based system-level simulation parameters

mMIMO-BSs	**Description**
Cellular layout	Wrap around hexagonal, 19 sites, 3 sectors/site
Deployment	Inter-site distance: 500 m, height: 32 m
Antenna array	Uniform linear, spacing: 0.5λ, Number of antennas per array: 64
Antenna pattern	70° H x 10° V beamwidths, 14 dBi max., downtilt: 15°
Precoder	Zero-forcing
Tx power/Noise figure	46 dBm, 5 dBm
Self-BH SCs	**Description**
Deployment	Random: $\{4, 8, 16\}$ SCs/sector, Ad-hoc: 16 SCs/sector, height: 5 m
Backhaul antenna pattern	5 dBi antenna gain, Omni
Access antenna pattern – Patch	80° H x 80° V beamwidths, 5 dBi max., downtilt: 90°
Access antenna pattern – Yagi	58° H x 47° V beamwidths, 10 dBi max., downtilt: 90°
Tx power/Noise figure	30 dBm, 5 dB
UEs	**Description**
Deployment	Random, 16 UEs/sector on average, all served, height: 1.5 m
Tx power/Noise figure	23 dBm, 9 dB
Channel	**Description**
Scenario	Outdoor SCs, outdoor UEs
Bandwidth/Time-slot	10 MHz at 2 GHz, $Q_t = 50$ RBs, $T = 1$ msec.
LoS probability, path loss and shadowing	• mMIMO-BS to UE (based on 3GPP macro to UE models as per [18]) • mMIMO-BS to SC (based on 3GPP macro to relay models as per [18]) • SC to UE (based on 3GPP relay to UE models as per [18])
Fast fading	Rician, distance-dependent K factor
Thermal noise	-174 dBm/Hz power spectral density

Therefore, the results for the average UE data-rate can be computed by numerical integration of (19).

In the next section, we will use this model to complement the insights given by the 3GPP-based system-level simulations.

V. Simulations and Numerical Results

In this section, we evaluate the performance of mMIMO s-BH and DA networks using 3GPP-based system-level simulations and mathematical analysis.

In the mMIMO s-BH network, the different characteristics of the backhaul and access radio links are modeled considering the methodology described in [18] for the 3GPP Case 1 Relay scenario. As described in [18, Tab. A.2.1.1.2-3], we adopt the LoS and NLoS path loss exponents $\eta^{\mathrm{L}} = 2.35$ and $\eta^{\mathrm{NL}} = 3.63$ for the backhaul links, and we consider $\eta^{\mathrm{L}} = 2.09$ and $\eta^{\mathrm{NL}} = 3.75$ for the access links. For each link, we use the corresponding LoS probability function proposed in [18, Tab. A.2.1.1.2-3]. To simulate the backhaul links, we account for the SC site planning correction factor, which affects the path loss and the LoS probability as indicated in [18, Tab. A.2.1.1.4-2]. To simulate the access links, we assume cross-correlated shadowing, with correlation coefficient $\rho = 0.5$ at the UE location with respect to the different SCs [18, Tab. A.2.1.1.2-3]. In the simulations, we consider a Rician fading model, and we characterize the Rician K-factor with the model: $K[\mathrm{dB}] = 13 - 0.03r$ in dB, where r is the distance between transmitter and receiver in meters [23].

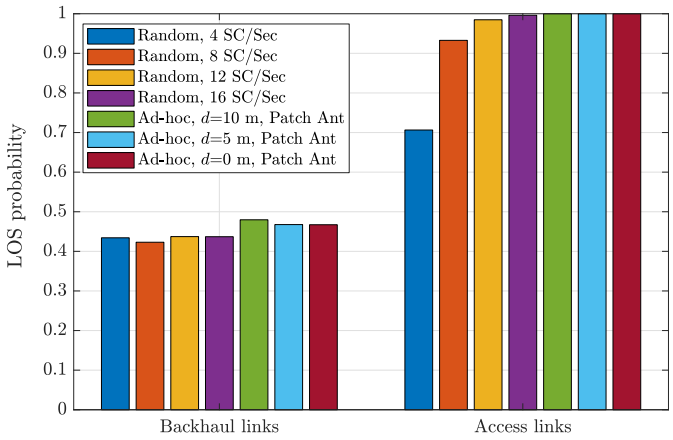

Fig. 3: LoS probability for SC backhaul links and UE access links in s-BH networks with Random and Ad-hoc deployments.

In the 3GPP-based system-level simulations, the channel gains (composed by path loss, shadowing and multi-path fading) are generated for all useful and interfering radio links between each SC and the UEs, as well as between each mMIMO-BS and all SCs. We collect statistics for different network realizations, each with independent deployments of UEs and SCs. Subsequently, we measure the performance in terms of the cumulative distribution functions (CDFs) of the backhaul SC rates in (5), of the access UE rates in (7), and of the end-to-end UE rates in (8).

To compare mMIMO s-BH against mMIMO DA architectures, we also simulate the links between mMIMO-BSs and UEs, and compute the resulting rates in (9). In the mMIMO DA network, we adopt the LoS probability function and the corresponding exponents $\eta^{\mathrm{L}} = 2.42$ and $\eta^{\mathrm{NL}} = 4.28$, as indicated in [18, Tab. A.2.1.1.2-3].

Table I contains the relevant parameters used to conduct the simulation campaign.

A. Massive MIMO s-BH: random vs. ad-hoc small cell deployments

In this subsection, we analyze the 3GPP-based simulation results for the two SC topologies described in Sec. II-A, namely the ad-hoc and random SC deployments. In both cases, $K_i = 16$ UEs are deployed per sector and scheduled in access time-slots by their serving SCs. We evaluate the impact of densification by considering $L_i = \{4, 8, 16\}$ SCs per sector for the case of random SC deployments. In the ad-hoc deployment, we consider $L_i = 16$ SCs per sector, and different values of the 2-D distance d from the UE to the SC. The resource partition α is set to 0.5, to distribute between backhaul and access the available resources equally.

As a first step, we compare the LoS probability of the backhaul and access links. The group of results in the left part of Fig. 3 shows the probability of a given SC to be in LoS with respect to the server mMIMO-BS with different densities of SCs and deployments. As expected, the percentages of backhaul links in LoS are almost the same in both the random and ad hoc deployments, since in the first case the SCs are randomly distributed with respect to mMIMO-BSs, while in the last approach the SCs are positioned in the vicinity of the UEs, which are randomly distributed with respect to mMIMO-BSs. Moreover, we can also see that the LoS probability of a UE in the s-BH architecture increases as the density of SCs increase, reaching 100% probability of LoS channel condition in the ad-hoc deployment, as shown by the results in the right part in Fig. 3. Overall, the backhaul link mainly limits the joint backhaul-access probability of LoS-LoS conditions.

As a second step, Figs. 4(a), 5(a) and 6 analyze the data-rate performance of the backhaul and access transmission by first considering the two links separately, and then their combined effect on the end-to-end UE rate. The following considerations can be made:

- *Backhaul link performance*: Fig. 4(a) illustrates the CDFs of the backhaul data-rates. These results show how increasing the number of SCs randomly deployed, and especially with the ad-hoc deployment, the backhaul data-rate received by each SC decreases. This is due to the reduction of the multiplying factor $\left[(M - L_a + 1)P_i^{\mathrm{dl}}\right]/L_a$ in (11), and the split of the transmit power among the active backhaul streams. It is worth to note that only the SCs with associated UEs are active (i.e. transmitting to the UEs), and are served via multiple backhaul links. Thus, looking at Fig. 4(b), which show the average number of SCs served by the mMIMO-BS when applying the random and ad-hoc SCs deployment strategies, we can better explain the results presented in Fig 4(a). In fact, while with the ad-hoc deployment almost all the 16 SCs are always active, with 16 randomly deployed SCs only 10 of them are active in average, as a result of the UEs association procedure. As depicted in Fig. 4(b), the analytical approximation in (10) of the SC activation probability matches the numerical results obtained by simulations.
- *Access link performance*: Fig. 5(a) shows the results for the access data-rate. As a general conclusion we can see that adding more randomly deployed SCs in the sector doesn't introduce a significant gain, while opportunistically deploying one SC closer to each UE is quite beneficial. In the following, we discuss the details of the different factors playing a key role in these results.
  On the one hand, when densifying the network, the carrier signal benefits from having SCs that are more likely in close vicinity to the served UE, even if a random SC deployment does not always guarantee this vicinity. Also, each SC has to serve a progressively reduced number of UEs in the access links (as indicated in Fig. 5(b)), and accordingly in the backhaul links, which means having more RBs available to allocate to each UE over different links.
  On the other hand, adding more SCs increases the probability of having a larger number of LoS interferers at the UE side. In the random deployment, the power of the interference links grows faster than the carrier signal power due to NLoS to LoS transition of the interference links [29]. In the ad-hoc case, the same interference effect takes place. However, by decreasing the distance d from UE to SC in such a way as to ensure that the position of the SC is always close to the served UE, the power

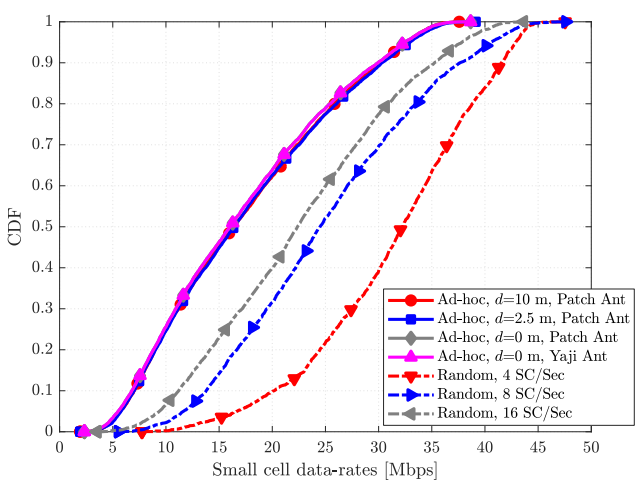

(a) CDF of SC rates for backhaul links

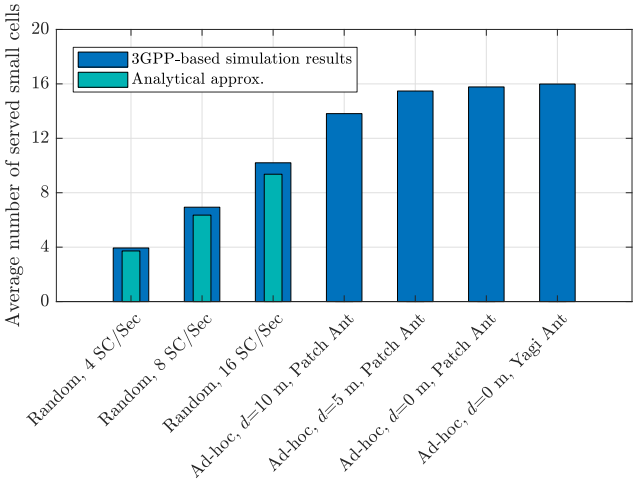

(b) Average number of SCs served per mMIMO-BS

Fig. 4: (a) CDF of SC rates for backhaul links, and (b) average number of SCs served in the backhaul time-slots. (b) also shows the analytical results for the SCs activation probability in (10).

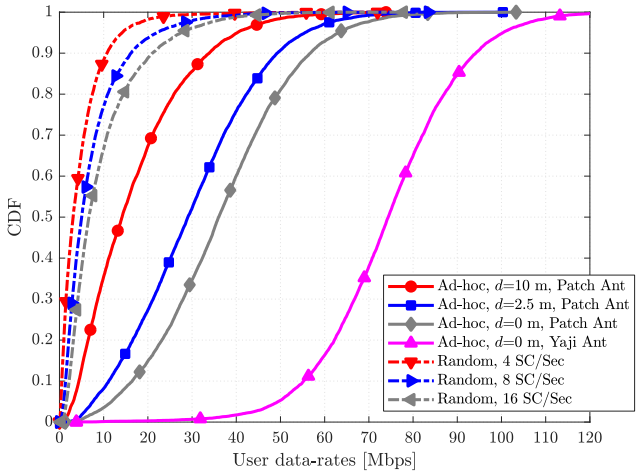

(a) CDF of UE rates for access links

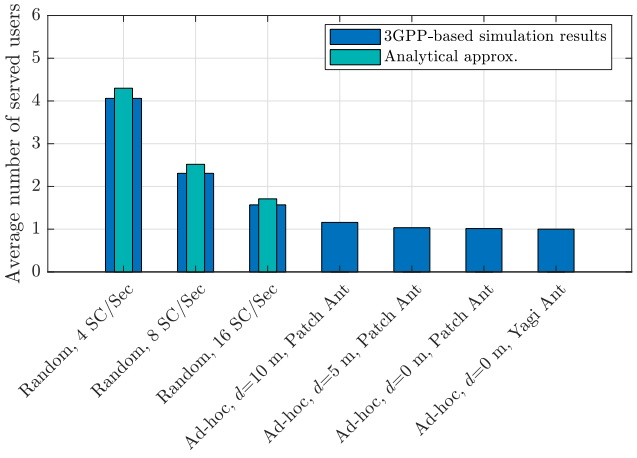

(b) Average number of UEs served per SC

Fig. 5: (a) CDF of UE rates for access links, and (b) average number of UEs served in the access time-slots. (b) also shows the analytical results for $\overline{K}$, i.e. the average number of UEs served per SC.

of the carrier signal increases faster than the interference power, and thus the hit in the SINR is not as significant. As a result, only a very dense deployment of random SCs could provide the same data-rate as in the case of the ad-hoc deployment. In subsection V-D, we will discuss the asymptotic behavior when increasing the density of SCs, and quantify the number of required randomly deployed SCs to achieve this condition.

From Fig. 5(a), we can observe how equipping the SC with a more directive antenna (i.e. Yagi) with respect to the Patch antenna further boosts the access link capacity to achieve 75 Mbps per UE at the median value. Two complementary effects cause this performance enhancement: *i)* the signal improvements provided by the higher antenna gain of the directive Yagi, and *ii)* the reduced interference created towards neighboring UEs served by other SCs.

- *End-to-end overall performance*: Fig. 6 shows the end-to-end results given by the combination of the two-hop, backhaul and access, performance previously depicted in Figs. 4(a) and 5(a). Overall, the end-to-end data-rates of the random deployment are more limited by the access links than by the backhaul links, as shown by comparing the results in Figs. 6 to the one in 5(a). On the contrary, the end-to-end data-rates of the ad-hoc deployment outperform the one of the random deployment, but are severely penalized by the backhaul links, as shown by comparing the results in Figs. 6 to the one in 4(a). Thus, the reduced backhaul capacity of the mMIMO sBH ad-hoc deployment does not fully allow to exploit the potentially high data-rate achieved in the access. This behavior suggests the need to optimize the splitting of resources between the two links. Indeed, a particularly important improvement in end-to-end rates would be achieved through the allocation of more resources to backhaul links. This is analyzed in the following section.

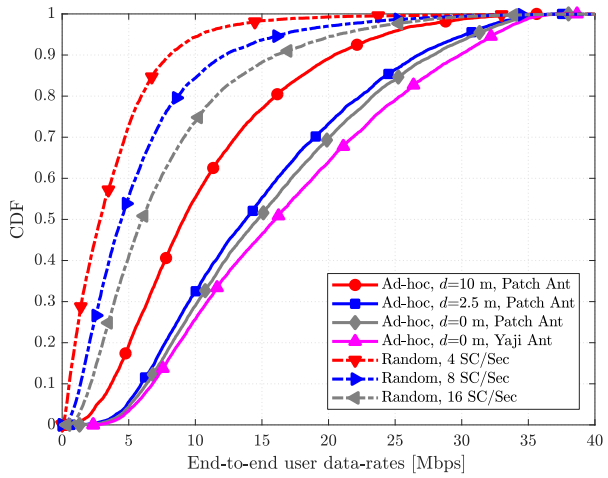

Fig. 6: CDF of end-to-end UE rates in: (i) ad-hoc deployment of 16 SCs per sector with variable UE-to-SC distance d, and (ii) random deployment of SCs.

B. Massive MIMO sBH: access and backhaul resource allocation

In Fig. 7, we vary α in the range $0 \leq \alpha \leq 1$, and analyze the behavior of UEs rate at the 5-th and 50-th percentiles of the CDF. The configurations $\alpha = 0$ and $\alpha = 1$ entail that all the time-slots are allocated to the access and the backhaul, respectively. Therefore, the UE rates for these two values are equal to 0, since no resources are left for the other link. Moreover, the configuration α^* represents the value of α that maximizes the UE rate. For instance, with $d = 0$ and Yagi antennas at the SCs, α^* is equal to 0.85 when looking at the 5-th percentile. Fig. 7 brings the following insights:

- By comparing the results between Fig. 7(a) and Fig. 7(b), it is important to note that the optimal α changes from 0.85 to 0.75. A tradeoff exists between 5-th and 50-th percentile performance, and they cannot be optimized simultaneously. Assuming that the network uses $\alpha = 0.85$, which is the optimal value for cell-edge UEs (5-th percentile of the CDF), the median UEs (50-th percentile of the CDF) can achieve an end-to-end rate of 19.5 Mbps, which represents a 16% reduction with respect to the maximum end-to-end rate achievable of 23.3 Mbps with $\alpha = 0.75$.
- In Figs. 7(a) and 7(b), we show with dashed lines the results of the mMIMO DA setup. A properly designed mMIMO s-BH radio resource partitioning can improve the performance of the cell-edge UEs, and keeps the same performance for the UEs at the median of the CDF with respect to mMIMO DA architecture, as shown in Figs. 7(a) and 7(b), respectively. A more detailed comparison is further developed in the next section.

C. Massive MIMO architectures: s-BH vs. direct access

First, we compare the joint probability of LoS-LoS channels in the backhaul-access legs for the s-BH network with the probability of LoS channel in the access links for the DA network. As shown in Fig. 8, there are higher joint backhaul-access LoS probabilities with respect to the access LoS

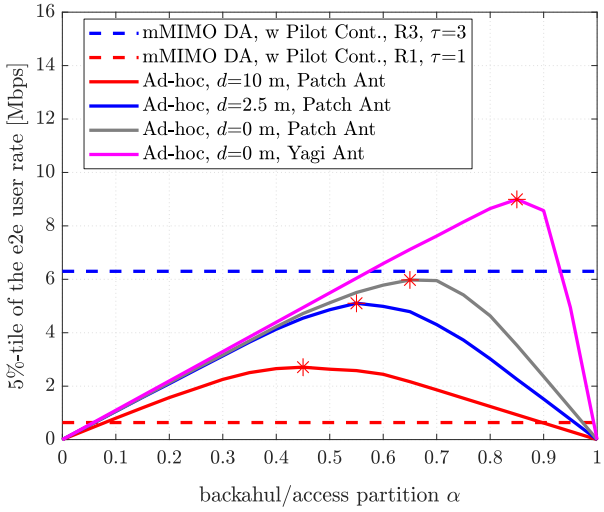

(a) 5-th percentile

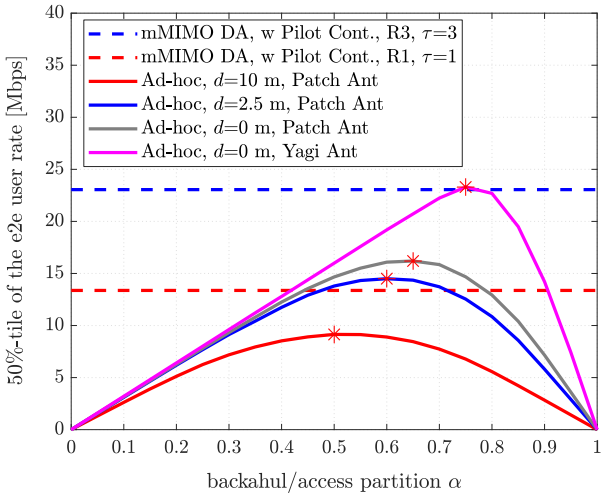

(b) 50-th percentile

Fig. 7: (a) 5-th, and (b) 50-th percentile of the end-to-end UE rates as a function of the fraction α of backhaul time-slots.

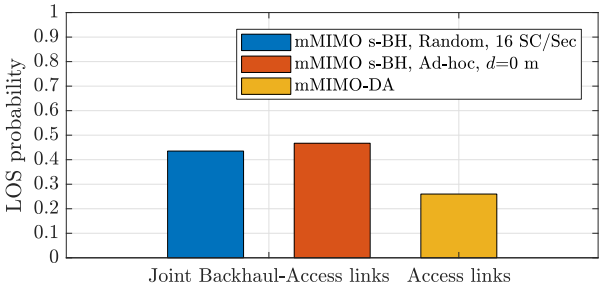

Fig. 8: LoS probability for joint backhaul-access links in s-BH network and for access links in DA network.

probability, 47% and 25%, respectively. Those are the cases where the s-BH architecture can potentially improve the UEs performance with respect to the DA architecture.

We also compare the end-to-end UE rates resulting from the 3GPP-based simulations of the mMIMO s-BH and mMIMO DA networks. As shown in Fig. 9, the mMIMO s-BH network with the ad-hoc deployment of SCs provides better perfor-

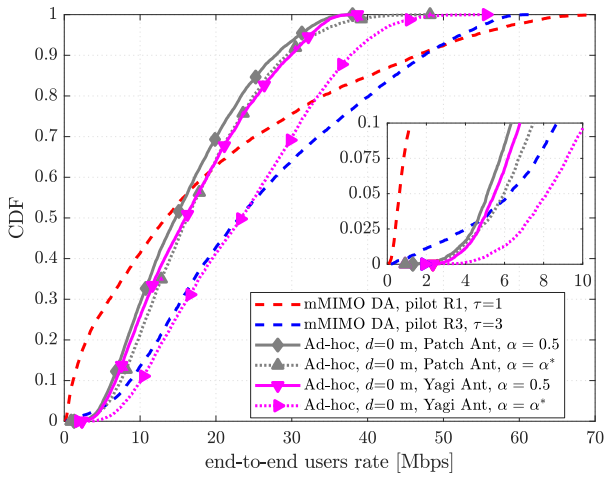

Fig. 9: Two types of curves are represented: (i) mMIMO DA with pilot reuse schemes 1 and 3; (ii) ad-hoc deployment of 16 SCs per sector for $\alpha = 0.5$ and $\alpha = \alpha^*$, at which the 50-th percentile of the end-to-end UE rate is maximized (as shown in Fig. 7(b)).

mance than the mMIMO DA network with pilot reuse 1 at the bottom of the CDF, i.e. below the 50-th percentile. In fact, pilot contamination severely degrades the rates of UEs at the cell edge in the mMIMO DA setup with pilot reuse 1. On the other hand, in the s-BH network, due to the longer coherence time of the static backhaul channel, T_{BH}, with respect to the system time-slot duration, T, there is no pilot contamination, and the UEs benefits from the proximity of SCs, which reduces the path loss and improves the LoS propagation condition, as shown in Fig. 8.

However, by adopting the pilot reuse 3 in the mMIMO DA network, the pilot contamination effect reduces, and the results show that the mMIMO DA performance exceeds the one of the mMIMO s-BH with $\alpha = 0.5$, even if the pilot overhead ($\tau = 3$ OFDM symbols) is 3 times larger with respect to pilot reuse 1. The mMIMO s-BH architecture provides the same performance as the mMIMO DA for the median UEs, only when the optimal partition $\alpha = \alpha^*$ is selected. Overall, mMIMO s-BH underperforms mMIMO DA above the median of the UE rates, and provides rate improvements for cell-edge UEs that amount to 30% and a tenfold gain when adopting pilot reuse 3 and reuse 1, respectively.

D. Asymptotic data-rate analysis

Figs. 10(a) and 10(b) show the convergence behavior of the backhaul and access data-rates for the random SCs deployment with respect to the results obtained with the ad-hoc deployment of 16 SCs, positioned at fixed distance $d = 0$ with respect to the UEs. In both cases the results are obtained by numerical integration of (16) and (19). Fig. 10(a) show the convergence results of the backhaul link. The backhaul data-rate of the random distribution (solid line) converges to the one of the ad-hoc (dashed line) when the number of SCs is 100 times larger than the number of ad-hoc SCs (denoted by the marker "*"). Fig. 10(b) shows the convergence results of the access link. In this case, the data rate of the random (solid line) converges to the ad-hoc (dashed line), when the number of SCs is 1000

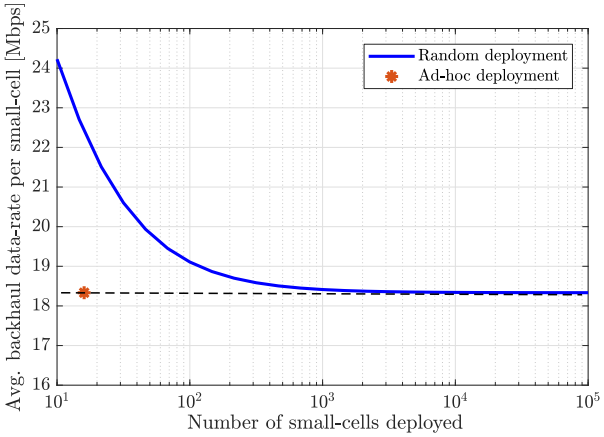

(a) Asymptotic SC data-rate for backhaul links

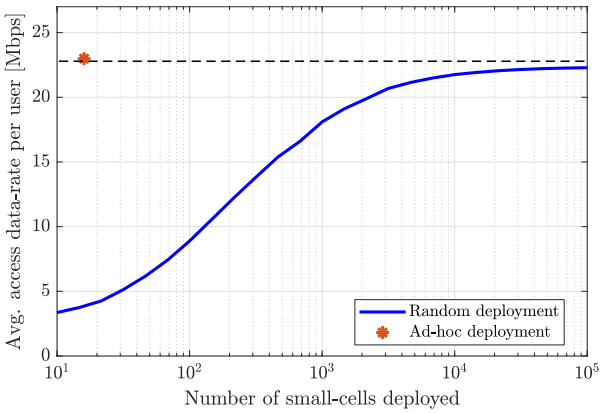

(b) Asymptotic UE data-rate for access links

Fig. 10: Asymptotic performance measures for backhaul and access links in s-BH network when random and ad-hoc deployments of SCs are considered.

times larger than the number of SCs deployed in the ad-hoc case (marker "*"). As shown in subsection V-B, the ad-hoc deployment is the one which maximizes the end-to-end data-rates of the two-hop communication.

The main takeaway is summarized by the possibility for the MNOs to explore the adoption of future dynamic SCs infrastructures better. Indeed, instead of significantly over-provisioning the number of SCs, it may be beneficial to dynamically reposition only the active ones, trying to guarantee the same performance that are obtained with a very dense deployment of SCs.

VI. Conclusion

In this paper, we studied the performance results for two 5G mMIMO architectures working at frequencies below 6 GHz: mMIMO s-BH and mMIMO DA. In the mMIMO s-BH architecture, we analyzed two different configurations: random deployment of SCs in the coverage area of the serving macro cell, and ad-hoc deployment of SCs in close proximity to each UE. Overall, we found that the random SCs distribution entails deploying thousands of SCs to achieve the capacity limit of the s-BH architecture. On the other hand, the ad-hoc deployment benefits from the close proximity of the SCs to the UEs, and outperforms the random one for reasonable

numbers of deployed SCs. However, the SC requires to know the UE position, and this is particularly complicated to realize due to mobility. Finally, we compared the performance of the mMIMO s-BH architecture to the one of the mMIMO DA. The former shows rate improvements for cell-edge UEs that amount to 30% and a tenfold gain when adopting pilot reuse 3 and reuse 1, respectively. Conversely, mMIMO DA outperforms mMIMO s-BH above the median of the UE rates, where the propagation conditions are more favorable.

REFERENCES

[1] A. Bonfante, L. Galati Giordano, D. López-Pérez, A. Garcia-Rodriguez, G. Geraci, P. Baracca, M. M. Butt, M. Dzaferagic, and N. Marchetti, "Performance of massive MIMO Self-Backhauling for Ultra-Dense small cell deployments," accepted to *2018 IEEE Global Telecomm. Conf. (Globecom 2018)*, Dec. 2018. [Online]. Available: https://arxiv.org/abs/1806.10969

[2] A. Gupta and R. K. Jha, "A survey of 5G network: Architecture and emerging technologies," *IEEE Access*, vol. 3, pp. 1206–1232, Jul. 2015.

[3] F. Rusek, D. Persson, B. K. Lau, E. G. Larsson, T. L. Marzetta, O. Edfors, and F. Tufvesson, "Scaling up MIMO: Opportunities and challenges with very large arrays," *IEEE Signal Processing Mag.*, vol. 30, no. 1, pp. 40–60, Jan. 2013.

[4] D. López-Pérez, M. Ding, H. Claussen, and A. H. Jafari, "Towards 1 Gbps/UE in cellular systems: Understanding ultra-dense small cell deployments," *IEEE Communications Surveys Tutorials*, vol. 17, no. 4, pp. 2078–2101, Fourthquarter 2015.

[5] U. Siddique, H. Tabassum, E. Hossain, and D. I. Kim, "Wireless backhauling of 5G small cells: challenges and solution approaches," *IEEE Wireless Communications*, vol. 22, no. 5, pp. 22–31, Oct. 2015.

[6] N. Wang, E. Hossain, and V. K. Bhargava, "Backhauling 5G small cells: A radio resource management perspective," *IEEE Wireless Communications*, vol. 22, no. 5, pp. 41–49, Oct. 2015.

[7] 3GPP TR 38.874, "Study on integrated access and backhaul," Technical Report (TR), May 2018.

[8] M. N. Kulkarni, J. G. Andrews, and A. Ghosh, "Performance of dynamic and static TDD in self-backhauled millimeter wave cellular networks," *IEEE Trans. Wireless Commun.*, vol. 16, no. 10, pp. 6460–6478, Oct. 2017.

[9] S. Singh, M. N. Kulkarni, A. Ghosh, and J. G. Andrews, "Tractable model for rate in self-backhauled millimeter wave cellular networks," *IEEE J. Sel. Areas Commun.*, vol. 33, no. 10, pp. 2196–2211, Oct. 2015.

[10] R. Gupta and S. Kalyanasundaram, "Resource allocation for self-backhauled networks with half-duplex small cells," in *2017 IEEE International Conference on Communications (ICC)*, May 2017, pp. 198–204.

[11] T. M. Nguyen, A. Yadav, W. Ajib, and C. Assi, "Resource allocation in two-tier wireless backhaul heterogeneous networks," *IEEE Trans. Wireless Commun.*, vol. 15, no. 10, pp. 6690–6704, Oct. 2016.

[12] A. Sharma, R. K. Ganti, and J. K. Milleth, "Joint backhaul-access analysis of full duplex self-backhauling heterogeneous networks," *IEEE Trans. Wireless Commun.*, vol. 16, no. 3, pp. 1727–1740, Mar. 2017.

[13] B. Li, D. Zhu, and P. Liang, "Small cell in-band wireless backhaul in massive MIMO systems: A cooperation of next-generation techniques," *IEEE Trans. Wireless Commun.*, vol. 14, no. 12, pp. 7057–7069, Dec. 2015.

[14] H. Tabassum, A. H. Sakr, and E. Hossain, "Analysis of massive MIMO-enabled downlink wireless backhauling for full-duplex small cells," *IEEE Trans. Commun.*, vol. 64, no. 6, pp. 2354–2369, Jun. 2016.

[15] H. H. Yang, G. Geraci, and T. Q. S. Quek, "Energy-efficient design of MIMO heterogeneous networks with wireless backhaul," *IEEE Trans. Wireless Commun.*, vol. 15, no. 7, pp. 4914–4927, Jul. 2016.

[16] M. Feng, S. Mao, and T. Jiang, "Joint frame design, resource allocation and user association for massive MIMO heterogeneous networks with wireless backhaul," *IEEE Trans. Wireless Commun.*, vol. 17, no. 3, pp. 1937–1950, Mar. 2018.

[17] Y. G. Lim, C. B. Chae, and G. Caire, "Performance analysis of massive MIMO for cell-boundary users," *IEEE Trans. Wireless Commun.*, vol. 14, no. 12, pp. 6827–6842, Dec. 2015.

[18] 3GPP 36.814, "Further advancements for E-UTRA physical layer aspects," Technical Report (TR), Mar. 2017.

[19] I. Bor-Yaliniz and H. Yanikomeroglu, "The new frontier in RAN heterogeneity: Multi-tier drone-cells," *IEEE Communications Magazine*, vol. 54, no. 11, pp. 48–55, Nov. 2016.

[20] J.-M. Kelif, M. Coupechoux, and P. Godlewski, "A fluid model for performance analysis in cellular networks," *EURASIP Journ. Wireless Commun. Network.*, vol. 2010, no. 435189, Aug. 2010.

[21] M. Minelli, M. Ma, M. Coupechoux, J. M. Kelif, M. Sigelle, and P. Godlewski, "Optimal relay placement in cellular networks," *IEEE Trans. Wireless Commun.*, vol. 13, no. 2, pp. 998–1009, Feb. 2014.

[22] C. Liu, M. Ding, C. Ma, Q. Li, Z. Lin, and Y. Liang, "Performance analysis for practical unmanned aerial vehicle networks with LoS/NLoS transmissions," *ArXiv e-prints*, vol. abs/1804.00811, Apr. 2018. [Online]. Available: http://arxiv.org/abs/1804.00811

[23] 3GPP 25.996, "Spatial channel model for Multiple Input Multiple Output (MIMO) simulations (Release 14)," Technical Report (TR), Mar. 2017.

[24] X. Zhu, Z. Wang, C. Qian, L. Dai, J. Chen, S. Chen, and L. Hanzo, "Soft pilot reuse and multicell block diagonalization precoding for massive MIMO systems," *IEEE Trans. Veh. Technol.*, vol. 65, no. 5, pp. 3285–3298, May 2016.

[25] H. Q. Ngo, E. G. Larsson, and T. L. Marzetta, "The multicell multiuser MIMO uplink with very large antenna arrays and a finite-dimensional channel," *IEEE Transactions on Communications*, vol. 61, no. 6, pp. 2350–2361, Jun. 2013.

[26] L. Galati Giordano, L. Campanalonga, D. López-Pérez, A. Garcia-Rodriguez, G. Geraci, P. Baracca, and M. Magarini, "Uplink sounding reference signal coordination to combat pilot contamination in 5G massive MIMO," in *2018 IEEE Wireless Communications and Networking Conference (WCNC)*, Apr. 2018, pp. 1–6.

[27] S. Lee and K. Huang, "Coverage and economy of cellular networks with many base stations," *IEEE Communications Letters*, vol. 16, no. 7, pp. 1038–1040, Jul. 2012.

[28] J. G. Andrews, R. K. Ganti, M. Haenggi, N. Jindal, and S. Weber, "A primer on spatial modeling and analysis in wireless networks," *IEEE Communications Magazine*, vol. 48, no. 11, pp. 156–163, Nov. 2010.

[29] M. Ding, P. Wang, D. López-Pérez, G. Mao, and Z. Lin, "Performance impact of LoS and NLoS transmissions in dense cellular networks," *IEEE Trans. Wireless Commun.*, vol. 15, no. 3, pp. 2365–2380, Mar. 2016.

[30] C. Galiotto, N. K. Pratas, N. Marchetti, and L. Doyle, "A stochastic geometry framework for LoS/NLoS propagation in dense small cell networks," in *2015 IEEE International Conference on Communications (ICC)*, Jun. 2015, pp. 2851–2856.

APPENDIX A

In the following, we derive the expression used to evaluate the rate coverage probability. The probability that the access SIR is greater than a threshold $\gamma_a = 2^{\frac{R_{th}}{K-1}} - 1$, which depends on the minimum target rate R_{th}, is expressed as [30]

$$\Pr\left[\mathrm{SIR}^{\mathrm{A}}(x) > \gamma_a\right] = \Pr\left[\frac{P_l^{\mathrm{dl}} G_b |g|^2 \beta^{\mathrm{L}}(x)}{I_{\mathrm{agg}}} > \gamma_a\right] \overset{(a)}{=} \mathscr{L}_{I_{\mathrm{agg}}}\left(\frac{\gamma_a}{P_l^{\mathrm{dl}} G_b \beta^{\mathrm{L}}(x)}\right), \quad (20)$$

where (a) follows from [29, eq. (54)] neglecting the thermal noise as the propagation in sub-6 GHz bands is interference-limited and $\mathscr{L}_{I_{\mathrm{agg}}}(s)$ represents the Laplace transform of I_{agg}, and is defined according to [29], [30] as follows

$$\mathscr{L}_{I_{\mathrm{agg}}}(s) = \exp\left(-2\pi\tilde{\lambda_b}\int_x^{+\infty} \frac{\Pr^{\mathrm{L}}(u)\, u}{1 + \left(s P_l^{\mathrm{dl}} G_b \beta^{\mathrm{L}}(u)\right)^{-1}} du\right) \times \exp\left(-2\pi\tilde{\lambda_b}\int_{x_1}^{+\infty} \frac{\left[1 - \Pr^{\mathrm{L}}(u)\right] u}{1 + \left(s P_l^{\mathrm{dl}} G_b \beta^{\mathrm{NL}}(u)\right)^{-1}} du\right), \quad (21)$$

where $x_1 = \left(\frac{A^{\mathrm{NL}}}{A^{\mathrm{L}}}\right)^{\eta^{\mathrm{NL}}-1} x^{\frac{\eta^{\mathrm{L}}}{\eta^{\mathrm{NL}}}}$ [30].

View publication stats